Stability of the ternary perovskites Sc₃*E*N (*E*=B,Al,Ga,In) from first principles

A. S. Mikhaylushkin,[1] C. Höglund,[2] J. Birch,[2] Zs. Czigány,[3] L. Hultman,[2] S. I. Simak,[1] B. Alling,[1] F. Tasnádi,[1] and I. A. Abrikosov[1]

[1]*Theory and Modeling Division, Department of Physics, Chemistry and Biology (IFM), Linköping University, S-581 83 Linköping, Sweden*

[2]*Thin Film Physics Division, Department of Physics, Chemistry and Biology (IFM), Linköping University, S-581 83 Linköping, Sweden*

[3]*Research Institute for Technical Physics and Materials Science, Hungarian Academy of Sciences, P.O. Box 49, H-1525 Budapest, Hungary*

Mechanical and thermodynamic stability of the isoelectronic ternary inverse perovskites Sc₃EN (*E* =B,Al,Ga,In) has been studied from first principles. We confirm stability of recently synthesized cubic phases Sc₃AlN and Sc₃InN, and predict the stability of cubic Sc₃GaN and a triclinic phase aP20-Sc₃BN. Substantial phonon softening in Sc₃AlN and Sc₃GaN is observed indicating a possibility that structural defects could form readily. In accord, our experiments show that magnetron sputter deposited films contain regions with high density of nonperiodic stacking faults along the ⟨111⟩ growth direction. We suggest that defect-free crystals may exhibit anomalies in the carrier properties, promising for electronic applications.

PACS number(s): 71.20.Lp, 71.15.Pd, 71.38.−k, 71.15.Mb

In the recent experimental studies by Höglund *et al.*[1] and M. Kirchner *et al.*,[2] synthesis of new perovskites Sc₃AlN and Sc₃InN was reported. These compounds belong to the type of anti- or inverse perovskites.[3] The structural framework of Sc₃AlN-type structure (see Fig. 1) consists of a metallic subsystem Sc₃Al, which forms Cu₃Au-like arrangement of atoms and a nitrogen atom added in a body-centered position. Each Al atom is coordinated by 12 Sc atoms and each N atom is coordinated by only 6 Sc atoms. There is a family of ternary nitrides known to form the inverse perovskite structure with the general formula R_3EN, where R and E elements represent groups 2 and 11–15, respectively.[4] Some of such perovskite phases are found for the transition or rare-earth metals and groups 11–15 on the R and E elements, respectively.[5,6] These perovskite nitrides are attractive materials due to the possibility of designing their electronic properties within the same crystal structure. In particular, by varying electron concentration it is possible to achieve different situations with electron excess (as in Ca₃AuN) or electron deficiency (as in Ca₃TlN) that must be mirrored in the physical behavior of the compounds. For instance, Ca₃AuN is an electronic conductor, whereas compounds with group 15 elements are designed as insulators or semiconductors, and compounds with group 14 elements form so-called deficient metals.[4] Such peculiar electronic trend makes the perovskite nitride family attractive for different material applications.

The search for new materials is a fascinating and complicated task. Plenty of technologically important materials have recently been synthesized due to dramatic advances in experimental techniques. Unfortunately, different factors, such as structural complexity and impurities, which are not taken into account during the synthesis, may lead to an ambiguous or even wrong interpretation of the crystal structure arrangements, especially in multicomponent systems (see, for instance, Ref. 7). On the other hand, first-principles calculations represent a powerful tool for assisting experiment in the search and expertise of new phases. In fact, theoretical calculations provide information about thermodynamic and mechanical stability of postulated materials at different conditions. However, until recently the majority of calculations were restricted in static simulations at zero temperature with neglecting effects of lattice dynamics.[8] Consequently, the very possibility of a mechanical instability of a considered compound, i.e., its instability with respect to certain collective motions of atoms in the system, was ignored, which sometimes led to a misinterpretation of results (see discussion in Ref. 9). Therefore we report on the importance of probing both mechanical and thermodynamic stabilities of experimentally synthesized phases by means of first-principles calculations.

In the present article we perform a series of first-principles calculations of the electronic structure, phonon-spectra, and molecular-dynamics (MD) [*ab initio* molecular dynamics (AIMD)] simulations of the ternary isoelectronic
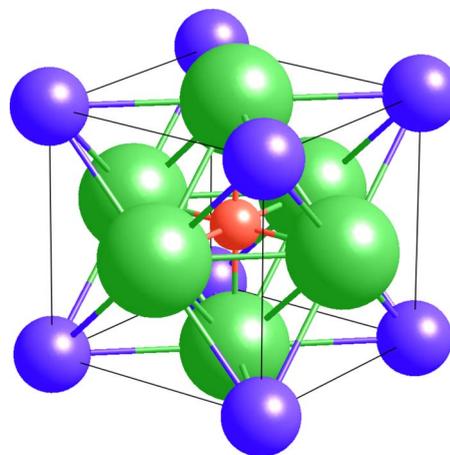

FIG. 1. (Color online) Crystal structure of the cubic inverse Sc₃AlN perovskite. Sc, Al, and N are marked by green (the largest circle), blue (the medium-sized circle), and red (the smallest circle) colors, respectively.

cubic perovskites Sc_3EN ($E=B, Al, Ga, In$) to analyze their mechanical and thermodynamic stabilities. We also analyze possible ways to stabilize the unstable phase Sc_3BN by applying appropriate structural distortions to the cubic structure.

The calculations were performed in the framework of the density-functional theory (DFT) (Ref. 10) using frozen core all-electron projector augmented wave (PAW) method,[11] as implemented in the program VASP.[12] This computational method has shown outstanding efficiency and reliability for the calculation of various physical properties and structural transformations of simple and complex materials.[13] Energy comparisons were performed by setting the same energy cut-off of 400 eV for all studied Sc_3EN. Exchange and correlation effects were treated within the generalized gradient approximation (GGA).[14] The $3p$, $3d$, and $4d$ semicore states of Sc, Ga, and In, respectively, were treated as valence. The integration over the Brillouin zone (BZ) was performed on a grid of special k points determined following the Monkhorst-Pack scheme.[15] For the cubic perovskite structure we used a grid of $16 \times 16 \times 16$ k points. For the distorted 40-atom structures the grid $6 \times 6 \times 6$ k point was used. Optimization of the volume and structural parameters, and atomic positions was done. Relaxation procedure of internal structural parameters and force calculations were performed within the Methfessel-Paxton scheme,[16] while the accurate total-energy calculations were carried out within the linear tetrahedron method with Blöchl's correction.[17] The total energies were converged to within 1 meV/atom.

Lattice parameters, calculated for cubic perovskites, are $a=4.24$ Å for Sc_3BN, $a=4.41$ Å for Sc_3AlN, $a=4.38$ Å for Sc_3GaN, and $a=4.46$ Å for Sc_3InN. Our results agree well with available experimental results for Sc_3AlN (Ref. 1) and Sc_3InN (Ref. 2).

We confirm the calculations of the band structure, density of states (DOS), and total energies with an all-electron full-potential method implemented in the FPLO7 package.[18] Exchange-correlation effects were treated within the Perdew-Wang[19] GGA for the exchange-correlation potential. The standard built-in basis functions were applied with the valence configurations of $(B:1s2s2p3s3p3d)$, $(N:1s2s2p3s3p3d)$, and $(Sc:3s3p4s3d4p5s4d)$. The 12 $\times 12 \times 12$ tetrahedral sampling in the k space led to convergence. More specific details can be found elsewhere.[20] Phonon-frequency calculations were done in the framework of the supercell approach (SCA) [small displacement method (SDM)] described in detail in Ref. 21. Forces induced by small atom displacements were calculated using the VASP program. We tested the convergence of the vibrational frequencies with respect to both the number of irreducible k points and the supercell size. To maintain the high accuracy we adopted $3 \times 3 \times 3$ supercells containing 135 atoms. The technique of phonon-spectra calculations was approved in our previous work.[22]

The first-principles molecular-dynamics simulation AIMD of the cubic and distorted structural arrangements of Sc_3EN were performed within the *NVT* canonical ensemble (*N*—number of atoms; *V*—volume; and *T*—temperature). The calculations of energies were done using the same PAW method, as for the electronic structure calculations. The su-
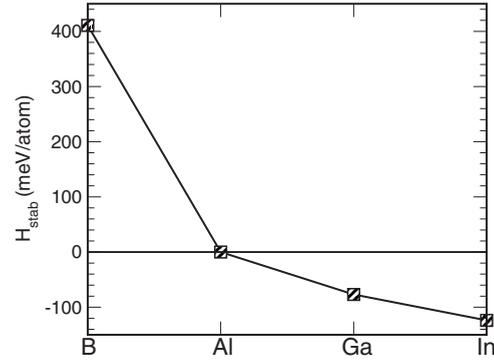

FIG. 2. Stabilization enthalpy [Eq. (1)] of cubic Sc_3EN ($E=B$, Al, Ga, and In) perovskite compounds.

percells for the AIMD simulations were adjusted to 40-atom cells. Tests of dynamical stability of solids within AIMD simulations require moderate accuracy of the electronic structure calculations but a very long computational time (see Ref. 23). Therefore for the MD runs we choose the k-point grid of $2 \times 2 \times 2$ k points for the integration over the BZ. We notice, however, that the latter change does not affect conclusions regarding the stability test. The temperature was set at 300 K. The smearing of the Fermi function was also set according to $T \sim 300$ K. The time step was equal to 1 fs. About 3000 time steps were performed for each AIMD run. In AIMD simulations the structural parameters a, b, and c were not changed.

Estimation of the thermodynamic stability of compounds is usually performed in terms of the formation enthalpy H_{form}, which by definition is the difference between the enthalpy of the compound and the enthalpies of its elemental components. However, in multicomponent alloy systems, the negative sign of H_{form} is not sufficient for stability since a possibility of decomposition of the compound into a mixture of more stable compounds needs to be considered. Thus, one needs to enumerate all possible competing phases and consider an energy balance for the possible decomposition reactions in the system of interest.

In Ref. 1 the estimation of the thermodynamic stability of cubic Sc_3AlN was carried out with respect to all known binary phases in the Sc-Al-N system. All calculated enthalpy differences were found to be negative. The mixing enthalpy (H_{mix}) of Sc_3AlN calculated with respect to ScN and $AlSc_2$ is -0.107 eV/atom. This indicated the thermodynamic stability of Sc_3AlN perovskite, in agreement with experiment.[1] To estimate the relative stability of three other perovskite compounds based on this result we calculate the stabilization enthalpies of Sc_3InN, Sc_3GaN, and Sc_3BN defined as the difference in formation enthalpies between these compound and Sc_3AlN,

$$H_{stab} = H_{form}(Sc_3EN) - H_{form}(Sc_3AlN), \qquad (1)$$

where formation enthalpy is calculated with respect to pure elements

$$H_{form} = H(Sc_3EN) - 3H(Sc) - H(Al) - \tfrac{1}{2}H(N_2).$$

Results of the calculations are shown in Fig. 2. One can

see that with increase in the period number of E elements in the Periodic Table, H_{stab} decreases. While H_{stab} has a positive sign for Sc$_3$BN, it is negative for Sc$_3$GaN and Sc$_3$InN, which indicates lower values of their formation enthalpies with respect to Sc$_3$AlN. In particular, H_{stab} of Sc$_3$InN is -0.11 eV/atom. We also carried out an additional estimation of the thermodynamic stability for Sc$_3$InN by calculation of its mixing enthalpy with respect to two thermodynamically stable phases in this system, ScN and InSc$_2$. This is the same procedure as was adopted for Sc$_3$AlN in Ref. 1. The obtained mixing enthalpy of the Sc$_3$InN is by 0.112 eV/atom lower than the corresponding mixing enthalpy of Sc$_3$AlN and agrees very well with the calculated stabilization enthalpy (cf. Fig. 2). Therefore we can further rely on the H_{stab} in our analyses of thermodynamic stability of compounds.

Interestingly, H_{stab} of Sc$_3$EN behaves almost linearly between E=In and Al, with H_{stab} of Sc$_3$GaN being situated between those of Sc$_3$InN and Sc$_3$AlN. Note that calculations indicate the thermodynamic stability of Sc$_3$AlN and Sc$_3$InN perovskites, in agreement with experiment.[1,2] This means that Sc$_3$GaN should also be stable. On the contrary, the value of H_{stab} of Sc$_3$BN is sufficiently higher than what could be expected from the linear trend of its heavier isoelectronic compounds. Therefore, one can expect that formation of Sc$_3$BN is thermodynamically unfavorable.

In order to draw a rigorous conclusion concerning stability of the family of perovskite compounds we examined their mechanical stability. Figure 3 shows calculated phonon spectra of the investigated perovskites. The spectrum of Sc$_3$BN indicates that this compound is mechanically unstable as phonon frequencies ω along the (110) and (111) directions become imaginary with minima at points M and R, respectively. This leads to the conclusion that the ideal stoichiometric Sc$_3$BN perovskite cannot exist in nature. On the contrary, the phonon frequencies in the spectra of the other perovskites, Sc$_3$AlN, Sc$_3$GaN, and Sc$_3$InN are all positive. This means that these compounds are mechanically stable and can exist at least in a metastable form. Thus, we conclude that apart from known perovskites Sc$_3$AlN and Sc$_3$InN, it may be possible to synthesize Sc$_3$GaN.

Phonon instabilities can be lifted by a formation of a charge-density wave (CDW) with a propagating k vector corresponding to the imaginary frequency, which results in displacements of atom positions along the propagation of a particular CDW in real space. This is particularly possible in case of locally manifested instability.[24] In the case of Sc$_3$BN, the instability of the phonon spectrum manifests itself around the high symmetry k vectors M and R.

At k-vector M, corresponding to the [110] direction the transverse phonon branch TA_1 has imaginary frequency values with polarization vectors [100] and [010] for Sc atoms in positions Sc1 ($\frac{1}{2}$ 0 $\frac{1}{2}$) and Sc2 (0 $\frac{1}{2}$ $\frac{1}{2}$), respectively. The general scheme (see, for example, Ref. 24) of the search of the mechanically stable structure is as follows. The five-atom cubic unit cell was doubled in all three dimensions. All atoms of Sc1 type neighboring in the [110] propagation directions were shifted mutually along polarization vectors [100] and [$\bar{1}$00]. Atoms of Sc2 types neighboring in the [110] propagation direction were shifted along the corresponding
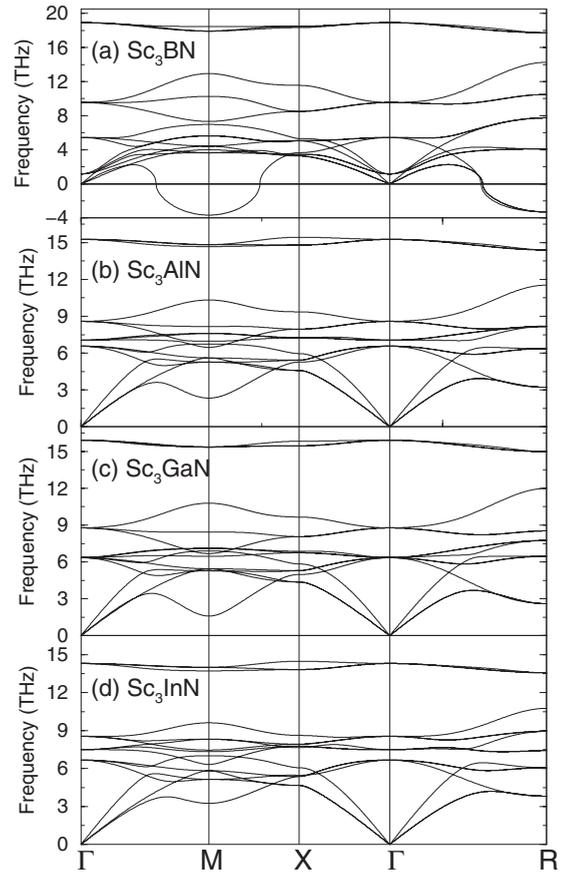

FIG. 3. Phonon spectra of (a) Sc$_3$BN, (b) Sc$_3$AlN, (c) Sc$_3$GaN, and (d) Sc$_3$InN. Negative values in (a) indicate imaginary frequencies.

polarization vectors [010] and [0$\bar{1}$0]. Such perturbations of Sc1 and Sc2 atoms reduce the symmetry of the 40-atom unit cell to tetragonal [Fig. 4(a)]. Though the frequency values at point M for both transverse branches are equal, we point out that the length of the distortion is not necessarily equal in the real space since a CDW may only indicate a direction for structural stabilization.[24] Consequently due to asymmetric distortions the symmetry of the unit cell may further reduce. In fact, after a procedure of structural relaxation the cell retained tetragonal symmetry. The unit cell can be reduced by symmetry to ten atoms with five inequivalent atomic positions (see Table I). The energy of this T-10 structure is lower than that of the cubic perovskite by 75 meV/atom.

In the same way we apply the CDW for the instability at k-vector R. In this case the direction of the CDW propagation is [111]. All three acoustic phonon branches have imaginary frequencies. The corresponding polarization vectors concern Sc atoms in positions Sc1 ($\frac{1}{2}$ 0 $\frac{1}{2}$), Sc2 (0 $\frac{1}{2}$ $\frac{1}{2}$), and Sc3 ($\frac{1}{2}$ $\frac{1}{2}$ 0). To adopt the cell to the distortions with the [111] propagation direction in real space, we double the cell in all three dimensions. Atoms of Sc1, Sc2, and Sc3, neighboring with atoms of the same type in the [111] propagation direction, were shifted mutually along the sum of three polarization vectors, corresponding to the three unstable phonon branches. For Sc1, Sc2, and Sc3 the sums of the polarization vectors are equal to vectors [101], [011], and [110], respec-
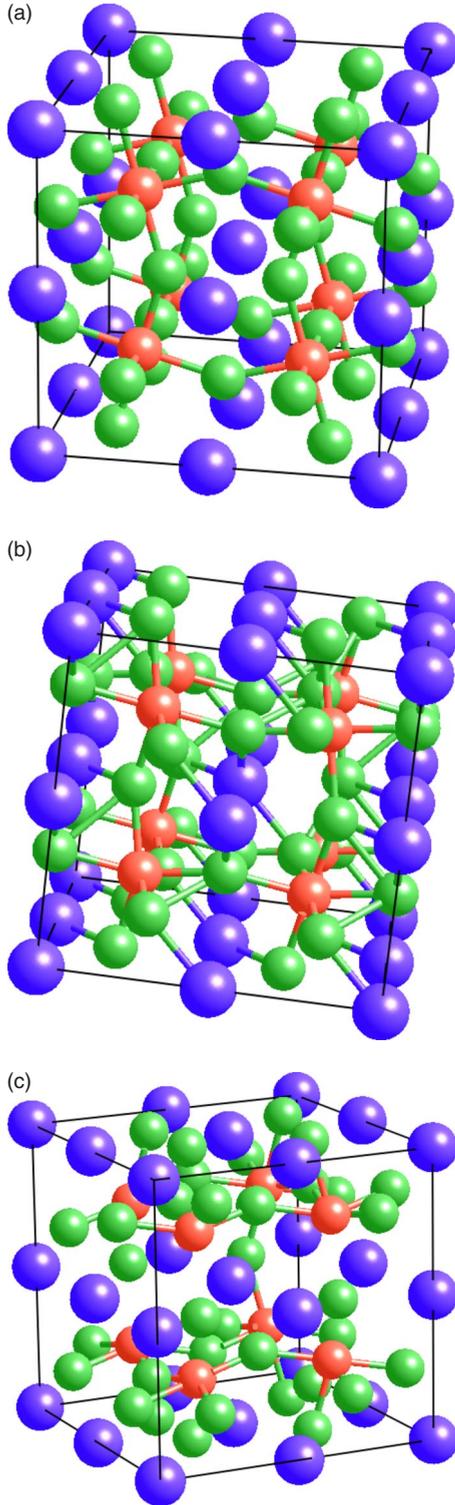
FIG. 4. (Color online) Crystal structures of Sc$_3$BN: T-10 (a), R-10 (b), and Tryck-20 (c). Blue atoms: B; green atoms: Sc; and red atoms: N.

TABLE I. Structural parameters of P-10 phase of Sc$_3$BN, tetragonal, and space group: $P4/mbm$ ($N=127$); $a=5.91$ Å, and $c=4.31$ Å.

	Basis vectors		
a	0.50000000	0.50000000	0.00000000
b	−0.50000000	0.50000000	0.00000000
c	0.00000000	0.00000000	0.51558976
	Atom positions in fractional coordinates		
Sc	0.17968593	0.17968593	0.50000000
Sc	−.17968593	−.17968593	0.50000000
Sc	−.32031407	0.32031407	0.50000000
Sc	0.32031407	−.32031407	0.50000000
Sc	0.00000000	0.50000000	0.00000000
Sc	0.50000000	0.00000000	0.00000000
B	0.00000000	0.00000000	0.00000000
B	0.50000000	0.50000000	0.00000000
N	0.00000000	0.50000000	0.50000000
N	0.50000000	0.00000000	0.50000000

atoms (see Table II). The energy of this R-10 structure is lower than that of the cubic one by 96 meV/atom.

The substantial change in the total energy upon structural distortion may imply mechanical stabilization. In fact, displacements of Sc atoms are characterized by decreasing Sc-B distances, which provides an optimization of the Sc-B bond length. However, we expect to obtain even more stable structures by simultaneous application of the CDW for the M and R k vectors. Corresponding atom displacements can be performed in the $2\times2\times2$ supercell of the initial five-atom cubic cell as a linear combination of two independent perturbations of the positions of Sc atoms [see Fig. 4(c)]. The initial supercell has now a base-centered orthorhombic sym-

TABLE II. Structural parameters of R-10 phase of Sc$_3$BN, triclinic, and space group: $P1$; $a=9.285$ Å, $b=5.842$ Å, $c=10.85$ Å, cos $\alpha=0$, cos $\beta=0.2078$, and cos $\gamma=0.943$.

	Basis vectors		
a	0.49924431	0.02621417	−.02564577
b	0.00000000	1.00000000	0.00000000
c	0.00000000	−0.02703954	0.49915690
	Atom positions in fractional coordinates		
Sc	−.40208476	0.10772179	0.05758045
Sc	0.36793523	0.37906979	0.05832843
Sc	−.22774929	0.47519999	−.34583316
Sc	0.23062933	−.02538785	0.42476294
Sc	−.36838437	−.11972499	0.42691477
Sc	0.40403956	−.39163685	−.34526114
Al	0.00004775	0.03921060	−.15707158
Al	0.00152673	−.46166065	−.15824671
N	0.00029891	0.24548994	0.01660561
N	0.00140144	−0.25534401	0.01587618

tively. The perturbations of the positions of the Sc atoms reduce the symmetry of the initial 40-atom unit cell structure [Fig. 4(b)], which we further address as R-10, to rhombohedral. After relaxation the symmetry reduces to triclinic $P1$ space group. The triclinic unit cell contains ten inequivalent

TABLE III. Structural parameters of aP20 phase of Sc$_3$BN, simple tetragonal, and space group: *P*1; *a*=5.66 Å, *b*=8.37 Å, *c*=6.227 Å.

Basis vectors			
a	0.74385179	0.00000000	0.000000
b	0.00000000	1.00000000	0.00000000
c	0.00000000	0.00000000	0.67615567
Atom positions in fractional coordinates			
Sc	0.18485030	−0.06217045	−0.18768475
Sc	−0.18485030	0.06217045	0.18768475
Sc	−0.18484610	0.43783157	0.18768194
Sc	0.18484610	−0.43783157	−0.18768194
Sc	0.31530244	−0.06217048	0.31233373
Sc	−0.31530244	0.06217048	−0.31233373
Sc	−.31530573	0.43782596	−.31233620
Sc	0.31530573	−0.43782596	0.31233620
Sc	0.12328042	0.24999786	−.45427005
Sc	−0.12328042	−0.24999786	0.45427005
Sc	0.37672688	0.24999873	0.04573800
Sc	−0.37672688	−0.24999873	−0.04573800
Al	−.03293838	0.25000369	−.08834010
Al	0.03293838	−0.25000369	0.08834010
Al	0.46683672	−.25000594	−.41160052
Al	−0.46683672	0.25000594	0.41160052
N	0.00000000	0.00000000	0.50000000
N	0.50000000	0.00000000	0.00000000
N	0.00000000	0.50000000	0.50000000
N	0.50000000	0.50000000	0.00000000

metry. After the relaxation procedure we obtained a structure with triclinic symmetry, which we name aP20. The supercell of aP20 can be reduced to a triclinic 20-atom unit cell. The structural parameters are shown in Table III. The aP20 structure has the lowest energy among all the considered Sc$_3$BN arrangements, 120 meV/atom lower than the cubic perovskite structure.

All three structural arrangements of Sc$_3$BN were examined with respect to mechanical stability. We notice that the crystal structures *T*-10, *R*-10, and, especially, aP20 are relatively complex for the phonon-spectra analyses. Therefore, to examine their mechanical stability the AIMD simulations were used. For that the cells of all structures were adjusted to 40-atom supercells and periodic boundary conditions were employed to describe long-range interactions. The AIMD runs were performed at room temperature for the duration of 6 ps. During the AIMD run after initial heating, a mechanically stable system would equilibrate and its atoms would oscillate around their initial positions. However atoms of a mechanically unstable system would not be able to oscillate around their initial positions; the system would "flow" trying to find a more favorable structural arrangement forbidden by symmetry or energy barriers. Consequently the structural instability would manifest itself in anomalous atom oscillations and abrupt changes in the diagonal elements of the stress

tensor (DEST) of the supercells.[23] Therefore we used DEST as an indicator of such instability. As an ultimate test we performed AIMD simulations also for the cubic inverse perovskite structure, which is already known to be mechanically unstable. During initial heating (300–500 steps) the AIMD runs of the cubic phase as well as *T*-10 and *R*-10 structures demonstrated strong variations in the DEST, features typical for mechanically unstable systems, and eventually atom positions drifted into another more stable structural arrangements. However, for aP20 the DEST behaved sufficiently smooth, indicating mechanical stability of the crystal structure. Therefore, we conclude that among *T*-10, *R*-10, and aP20, only aP20 is dynamically stable. We further analyzed the resulting structural arrangements of the AIMD runs from initial cubic, *T*-10, and *R*-10 structures. We found that their fractional coordinates are similar to those of aP20. When performing relaxation of the shape parameters, we obtained the aP20 structure. In this way we established mechanical stability of the most stable distorted structural arrangement within two independent first-principles techniques. By separate applications of two CDWs we obtained mechanically unstable structural arrangements *T*-10 and *R*-10, whereas only by simultaneous application of two CDW, it became possible to stabilize the Sc$_3$BN in a distorted aP20 structure.

Our combined analyses of the total energy and mechanical stability give evidence of three mechanically stable cubic inverse perovskites Sc$_3$AlN, Sc$_3$GaN, and Sc$_3$InN, as well as the distorted aP20 structure in Sc$_3$BN system. We have to notice that mechanical stability, as well as relative stability of these compounds, does not guarantee their thermodynamic stability with respect to all possible variations in concentrations or structural frameworks, or dissociation to elemental materials. Nevertheless, as soon as such a phase is obtained by epitaxial growth as Sc$_3$AlN, by arc melting as Sc$_3$InN, by compression, etc, a phase can exist in a metastable form at ambient condition. In our work we not only confirm structural stability of the already synthesized cubic inverse perovskites Sc$_3$AlN and Sc$_3$InN but also predict such a structure in Sc$_3$GaN and the distorted aP20 phase in Sc$_3$BN.

Electronic structure of the isoelectronic Sc$_3$EN systems is very similar (Fig. 5). All of the compounds demonstrate metallic behavior. The conducting electrons around the Fermi level (E_f) belong mainly to Sc 3*d* and 4*s* states, partly hybridized with each other (cf. Fig. 6). The valence states of Al and N are situated about 1 eV below the Fermi level. The valence states are separated from the semicore states by a pseudogap in Sc$_3$AlN and Sc$_3$GaN and by a small gap in Sc$_3$GaN (at about −0.8 eV). The bonding and antibonding states of Al and N atoms are separated by an energy gap of about 1.5 meV (see Fig. 6). Interestingly, in these particular compounds there is no hybridization between Sc states and Al or B states near the Fermi level, and on the contrary, the strong hybridization exists at −1 eV. The electronic conductivity is formed by an excess of Sc electrons. The DOS of the aP20 Sc$_3$BN is different. A gap between the bonding and antibonding states in B and N increases. The rearrangement of the Sc atoms in the distorted aP20 structure results in the appearance of the gap also in the Sc electronic subsystem below the Fermi level. This gap indicates an enhancement of the hybridization between the Sc and B due to the distortions in the aP20 structure.
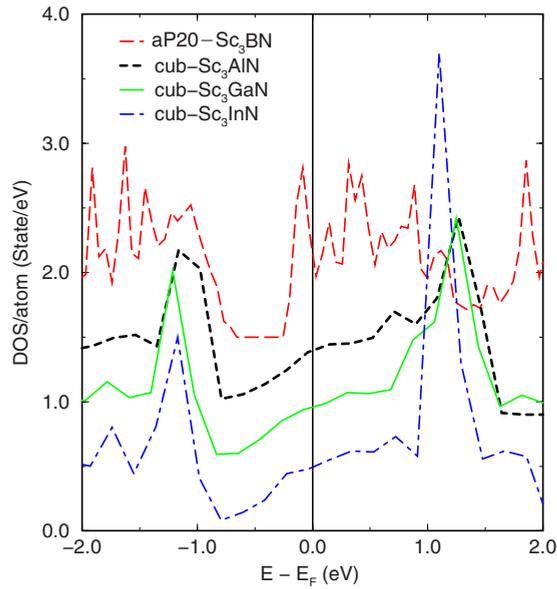
FIG. 5. (Color online) Electronic density of states (DOS) of cubic Sc$_3$EN (E=Al, Ga, In) and Tryck-20 Sc$_3$BN. The values of DOS for different compounds are shifted.

In general the peculiar electronic situation, realized in the compounds of Sc$_3$EN (E=B, Al, Ga, and In), can classify them as the electronic conductors with the *d*-state conductivity. Interestingly, it seems that the semicore and valence elec-
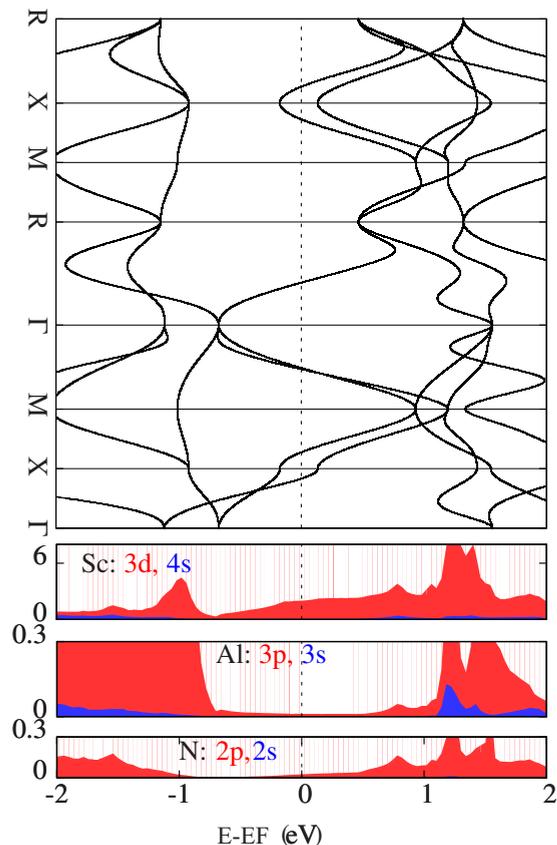

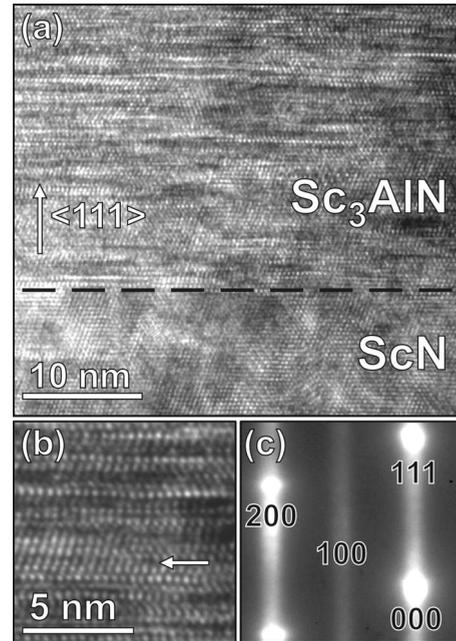FIG. 6. (Color online) Band structure and partial DOS of Sc$_3$AlN

FIG. 7. XTEM images from a Sc$_3$AlN(111) film sputter deposited on a ScN(111) seed layer on MgO(111) substrate (not shown). (a) The overview (the dash line shows the interface between seed layer and Sc$_3$AlN), (b) a higher magnification (the arrow depicts a dislocation), and (c) selected area electron-diffraction pattern.

trons are not interacting, and therefore variation in the elemental content and electronic occupations on Sc or Al may result only in effective change in the electronic concentration in the effectively noninteracting medium leading to a different electronic behavior: electronic conductors, semiconductors, or insulators as shown in Ref. 4.

For the dynamically stable cubic inverse perovskites we observe a pronounced softening of the phonon spectra around points *M* and *R* of the Brillouin zone. The softening of the phonon branches is strongest in Sc$_3$AlN and Sc$_3$GaN, while in Sc$_3$InN it is rather weak. Note that the trend of H_{stab} discussed above is in accord with the development of the softening of the vibrational branches in Sc$_3$EN phonon spectra. It is well known that such a phonon softening can influence the properties of electronic carriers or structural stability of compounds. Originated from Kohn singularity, softening of the vibrational spectra may result in anomalies of the elastic constants, enhancement of superconductivity,[25] ferroelectric properties,[26] shape-memory effects,[27] etc.

In order to investigate the consequences of the phonon softening in Sc$_3$AlN, the theoretical studies were complemented with experimental measurements of its conductivity and structural properties. The samples were prepared as in Ref. 1 and studied by cross-sectional transmission electron microscopy (XTEM), using FEI Tecnai G^2 TF 20 UT FEG and Philips CM20 microscopes, operated at 200 keV. The epitaxial Sc$_3$AlN films exhibited metallic conductivity, which agree with the results of our theoretical calculations. We did not observe any anomalies of conductivity in these samples above 10 K. At the same time, we observed that the magnetron sputter deposited films in Ref. 1 contained regions with high densities of structural defects. This is shown in Fig. 7(a)

where a Sc_3AlN film on a ScN seed layer is shown in XTEM. The Sc_3AlN films exhibit a high density of nonperiodic stacking faults along the $\langle 111 \rangle$ growth direction, in comparison with the close-to-perfect stacking in ScN. In Fig. 7(b) the irregular stacking of Sc_3AlN in the $\langle 111 \rangle$ direction is shown at higher magnification. The arrow in the image points at a dislocation which is a possible source for stacking faults. The streaks along the growth direction in the selected area electron-diffraction pattern of the film, taken along the $[0\bar{1}1]$ zone axis, shown in Fig. 7(c), confirm that the film contains stacking faults on the $\{111\}$ planes. The observed high defect density, which may be a consequence of the phonon softening on its own, can prevent the material from exhibiting electronic anomalies. In order to establish the physical properties of synthesized Sc_3AlN and predicted Sc_3GaN it is therefore imperative to grow crystals with fewer defects.

In summary, our first-principles calculations confirm the stability of the recently synthesized inverse perovskite

Sc_3AlN (Ref. 1) and Sc_3InN.[2] Via the analysis of the stabilization enthalpy and mechanical stability, we also predict the possibility of synthesizing the isoelectronic cubic perovskite Sc_3GaN and the distorted aP20 phase in Sc_3BN. The softening of the vibrational spectra in Sc_3AlN and Sc_3GaN compounds implies the presence of potentially intriguing physical properties, but their observation requires defect-free crystals to be grown.

¹C. Höglund, J. Birch, M. Beckers, B. Alling, Z. Czigány, A. Mücklich, and L. Hultman, Eur. J. Inorg. Chem. **2008**, 1193 (2008).

²M. Kirchner, W. Schnelle, F. R. Wabner, and R. Niewa, Solid State Sci. **5**, 1247 (2003).

³J. C. Schuster and J. Bauer, J. Solid State Chem. **53**, 260 (1984).

⁴See J. Jäger, D. Stahl, P. C. Schmidt, and R. Kniep, Angew. Chem. **105**, 738 (1993); Angew. Chem., Int. Ed. Engl. **32**, 709 (1993); D. A. Papaconstantopoulos and W. E. Pickett, Phys. Rev. B **45**, 4008 (1992); F. Gäbler, M. Kirchner, W. Schnelle, U. Schwarz, M. Schmitt, H. Rosner, and R. Niewa, Z. Anorg. Allg. Chem. **630**, 2292 (2004); R. Niewa, W. Schnelle, and F. R. Wagner, Z. Anorg. Allg. Chem. **627**, 365 (2000); E. O. Chi, W. S. Kim, N. H. Hur, and D. Jung, Solid State Commun. **121**, 309 (2002); Gäbler and R. Niewa, Inorg. Chem. **46**, 859 (2007).

⁵M. Barberon, R. Madar, E. Fruchart, G. Lorthioir, and R. Fruchart, Mater. Res. Bull. **5**, 1 (1970).

⁶See, for example, R. Benz and W. H. Zachariasen, Acta Crystallogr., Sect. B: Struct. Crystallog. Cryst. Chem **26**, 823 (1970).

⁷E. Gregoryanz, C. Sanloup, M. Somayazulu, J. Badro, G. Fiquet, H.-K. Mao, and R. J. Hemley, Nature Mater. **3**, 294 (2004); L. H. Yu, K. L. Yao, Z. L. Liu, and Y. S. Zhang, Physica B **399**, 50 (2007).

⁸See, for example, R. de Paiva, R. A. Nogueira, and J. L. A. Alves, Phys. Rev. B **75**, 085105 (2007); C. Paduani, J. Magn. Magn. Mater. **278**, 231 (2004); J. Von Appen, Angew. Chem., Int. Ed. **44**, 1205 (2005).

⁹E. I. Isaev, S. I. Simak, I. A. Abrikosov, R. Ahuja, Y. K. Vekilov, M. I. Katsnelson, A. I. Lichtenstein, and B. Johansson, J. Appl. Phys. **101**, 123519 (2007); A. F. Young, C. Sanloup, E. Gregoryanz, S. Scandolo, R. J. Hemley, and H. K. Mao, Phys. Rev. Lett. **96**, 155501 (2006).

¹⁰P. Hohenberg and W. Kohn, Phys. Rev. **136**, B864 (1964); W. Kohn and L. J. Sham, *ibid.* **140**, A1133 (1965).

¹¹P. E. Blöchl, Phys. Rev. B **50**, 17953 (1994); G. Kresse and D. Joubert, *ibid.* **59**, 1758 (1999).

¹²G. Kresse and J. Hafner, Phys. Rev. B **48**, 13115 (1993); G.

Kresse and J. Furthmüller, Comput. Mater. Sci. **6**, 15 (1996).

¹³B. Grabowski, T. Hickel, and J. Neugebauer, Phys. Rev. B **76**, 024309 (2007); A. S. Mikhaylushkin, U. Haussermann, B. Johansson, and S. I. Simak, Phys. Rev. Lett. **92**, 195501 (2004); A. S. Mikhaylushkin, S. I. Simak, B. Johansson, and U. Häussermann, J. Phys. Chem. Solids **67**, 2132 (2006); U. Häussermann, Chem.-Eur. J. **9**, 1471 (2003); U. Häussermann, O. Degtyareva, A. S. Mikhaylushkin, K. Soderberg, S. I. Simak, M. I. McMahon, R. J. Nelmes, and R. Norrestam, Phys. Rev. B **69**, 134203 (2004); A. S. Mikhaylushkin, S. I. Simak, B. Johansson, and U. Häussermann, *ibid.* **72**, 134202 (2005); A. S. Mikhaylushkin, J. Nylén, and U. Häussermann, Chem.-Eur. J. **11**, 4912 (2005); A. E. Kochetov and A. S. Mikhaylushkin, Eur. Phys. J. B **61**, 441 (2008); A. S. Mikhaylushkin, T. Sato, S. Carlson, S. I. Simak, and U. Haussermann, Phys. Rev. B **77**, 014102 (2008); A. Tenga, F. J. Garcia-Garcia, A. S. Mikhaylushkin, B. Espinosa-Arronte, M. Andersson, and U. Haussermann, Chem. Mater. **17**, 6080 (2005).

¹⁴Y. Wang and J. P. Perdew, Phys. Rev. B **44**, 13298 (1991); J. P. Perdew, J. A. Chevary, S. H. Vosko, K. A. Jackson, M. R. Pederson, D. J. Singh, and C. Fiolhais, *ibid.* **46**, 6671 (1992).

¹⁵H. J. Monkhorst and J. D. Pack, Phys. Rev. B **13**, 5188 (1976).

¹⁶M. Methfessel and A. T. Paxton, Phys. Rev. B **40**, 3616 (1989).

¹⁷P. E. Blöchl, O. Jepsen, and O. K. Andersen, Phys. Rev. B **49**, 16223 (1994).

¹⁸K. Koepernik and H. Eschrig, Phys. Rev. B **59**, 1743 (1999).

¹⁹J. P. Perdew and Y. Wang, Phys. Rev. B **45**, 13244 (1992).

²⁰FPLO7, see http://www.fplo.de and references therein.

²¹G. Kresse and J. Furthmuller, Europhys. Lett. **32**, 729 (1995); A. van de Walle and G. Ceder, Rev. Mod. Phys. **74**, 11 (2002) See homepage of D. Alfe for details, http://chianti.geol.ucl.ac.uk/~dario

²²L. Dubrovinsky, N. Dubrovinskaia, W. A. Crichton, A. S. Mikhaylushkin, S. I. Simak, I. A. Abrikosov, J. S. de Almeida, R. Ahuja, W. Luo, and B. Johansson, Phys. Rev. Lett. **98**, 045503 (2007); L. Dubrovinsky, N. Dubrovinskaia, O. Narygina, I. Kantor, A. Kuznetzov, V. B. Prakapenka, L. Vitos, B.

Johansson, A. S. Mikhaylushkin, S. I. Simak and I. A. Abrikosov, Science **316**, 1880 (2007); A. B. Belonoshko, L. Burakovsky, S. P. Chen, B. Johansson, A. S. Mikhaylushkin, D. L. Preston, S. I. Simak, and D. C. Swift, Phys. Rev. Lett. **100**, 135701 (2008); A. S. Mikhaylushkin, S. I. Simak, L. Burakovsky, S. P. Chen, B. Johansson, D. L. Preston, D. C. Swift, and A. B. Belonoshko, *ibid.* **101**, 049602 (2008); A. S. Mikhaylushkin, U. Haussermann, B. Johansson, and S. I. Simak, *ibid.* **92**, 195501 (2004); A. S. Mikhaylushkin, S. I. Simak, L. Dubrovinsky, N. Dubrovinskaia, B. Johansson, and I. A. Abrikosov, *ibid.* **99**, 165505 (2007).

²³ A. B. Belonoshko, E. I. Isaev, N. V. Skorodumova, and B. Johansson, Phys. Rev. B **74**, 214102 (2006), and references therein; C. Asker, A. B. Belonoshko, A. S. Mikhaylushkin, and I. A. Abrikosov, *ibid.* **77**, 220102(R) (2008).

²⁴ K. Persson, M. Ekman, and V. Ozolins, Phys. Rev. B **61**, 11221 (2000); A. S. Mikhaylushkin, S. I. Simak, B. Johansson, and U. Haussermann, *ibid.* **76**, 092103 (2007).

²⁵ H. Gutfreund, B. Horovitz, and M. Weger, J. Phys. C **7**, 383 (1974); D. Kasinathan, J. Kunes, A. Lazicki, H. Rosner, C. S. Yoo, R. T. Scalettar, and W. E. Pickett, Phys. Rev. Lett. **96**, 047004 (2006).

²⁶ W. Cochran, Phys. Rev. Lett. **3**, 412 (1959); P. W. Anderson and E. Blount, *ibid.* **14**, 217 (1965).

²⁷ K. Otsuka and X. Ren, Mater. Sci. Eng., A **273-275**, 89 (1999); M. J. Kelly and W. M. Stobbs, Phys. Rev. Lett. **45**, 922 (1980).